






# Next-Generation O-Band Coherent Transmission for 1.6 Tbps 10 km Intra-Datacenter Interconnects

Essam Berikaa , Graduate Student Member, IEEE, Md Samiul Alam , Graduate Student Member, IEEE, Santiago Bernal, Ramón Gutiérrez-Castrejón , Senior Member, IEEE, Weijia Li , Graduate Student Member, IEEE, Yixiang Hu , Graduate Student Member, IEEE, Benjamin Krueger, Fabio Pittalà, and David V. Plant, Fellow, IEEE

(Post-Deadline Paper)

## I. INTRODUCTION

**Abstract**—With the exponential growth of internet traffic, driven by the increasing number of connected devices and data-intensive applications, there is an urgent need to address the surging demand for higher capacity in datacenter communications. This article proposes using O-band single-carrier coherent transmission to achieve 1.6 Tbps for intra-datacenter reach (2–10 km), leveraging the advancements in next-generation DACs and the TFLN platform. To support our proposal, we assess experimentally the gain of employing 256 GSa/s interleaved DACs compared to the current state-of-the-art 128 GSa/s DACs. Additionally, we explore the feasibility of utilizing cost-effective DFB lasers in these short-reach systems. Using the 128 GSa/s DAC and DFB lasers, we transmit 120 Gbaud DP-64QAM over 10 km of SSMF under the 20% overhead SD-FEC threshold, featuring a net rate of 1.2 Tbps. Switching to 256 GSa/s DAC, we achieve net 1.6 Tbps transmission over 10 km with 167 Gbaud DP-64QAM below the 25% SD-FEC BER threshold. We observe that the power penalty of using DFB lasers compared to ECLs is less than 1 dB. Furthermore, this study includes a comprehensive analysis of the power consumption envelope for various candidate configurations targeting 1.6 Tbps operation. The comparison reveals the competitiveness of the O-band single-carrier coherent solution, attributed to its simpler architecture and the inherent features of the TFLN platform. The analysis highlights the potential of the proposed solution as a power-efficient and high-performance option for meeting the demanding requirements of 1.6 Tbps Ethernet.

**Index Terms**—Coherent communications, datacenter interconnects, O-band coherent transmission, optical fiber communication, power consumption, thin-film lithium niobate.

Manuscript received 31 May 2023; revised 25 July 2023; accepted 19 August 2023. Date of publication 22 August 2023; date of current version 2 February 2024. This work was supported by the Fonds de Recherche du Québec—Nature et Technologies under Grant 320758. (Corresponding author: Essam Berikaa.)

Essam Berikaa, Md Samiul Alam, Santiago Bernal, Weijia Li, Yixiang Hu, and David V. Plant are with the Photonic Systems Group, Department of Electrical and Computer Engineering, McGill University, Montréal, QC H3A 0E9, Canada (e-mail: essam.berikaa@mail.mcgill.ca; md.samiul.alam@mail.mcgill.ca; santiago.bernal@mail.mcgill.ca; weijia.li3@mail.mcgill.ca; yixiang.hu@mail.mcgill.ca; david.plant@mcgill.ca).

Ramón Gutiérrez-Castrejón is with the Photonic Systems Group, Department of Electrical and Computer Engineering, McGill University, Montréal, QC H3A 0E9, Canada, and also with the Institute of Engineering, Universidad Nacional Autónoma de México (UNAM), 04510 Mexico City, Mexico (e-mail: rgutierrezc@ingen.unam.mx).

Benjamin Krueger and Fabio Pittalà are with the Keysight Technologies GmbH, 130 71034 Böblingen, Germany (e-mail: benjamin.krueger@keysight.com; fabio.pittalà@keysight.com).

Color versions of one or more figures in this article are available at <https://doi.org/10.1109/JLT.2023.3307504>.

Digital Object Identifier 10.1109/JLT.2023.3307504

TO ADDRESS the surging traffic demand in intra-datacenter communications, particularly over distances of 2 to 10 km, dispersion-tolerant coherent transmission systems are being considered as an alternative to intensity modulation direct detection (IMDD) systems. While IMDD systems currently serve as the standard for applications up to 2 km at 200 Gbps/λ [1], their capacity scaling is severely limited by chromatic dispersion, even when operating in O-band. In IMDD systems, increasing the symbol rate or transmission reach is challenging due to the accumulated dispersion on the edge channels of the coarse wavelength division multiplexing (CWDM) grid (i.e., 1270 nm and 1330 nm). On the other hand, coherent transmission is resilient to dispersion and scales better with symbol rate, making it more suited to accommodate the escalating data traffic demand. Despite initial concerns regarding the added complexity and power consumption of coherent systems, the continued scaling of CMOS technology from 7 to 3 nm suggests that the ASIC power consumption envelope for both IMDD and coherent transceivers will potentially converge [2], [3]. Moreover, the IEEE 802.3 Ethernet Task Forces are currently investigating 800 G and 1.6 T capacity systems based on both IMDD and coherent transceiver architectures [4].

Operating in the O-band and employing coherent transmission techniques optimally fulfills several system objectives, as outlined below:

- 1) The capacity can be scaled by increasing the symbol rate as it is not limited by chromatic dispersion.
- 2) Optical amplification is unnecessary for distances up to 10 km, thereby reducing system complexity.
- 3) Digital dispersion compensation is not required in the receiver's digital signal processing (DSP) stack, simplifying the DSP architecture.
- 4) In the absence of dispersion, equalization-enhanced phase noise (EPPN) diminishes.
- 5) Feasibility of utilizing cost-effective distributed-feedback (DFB) lasers with relaxed linewidth requirements.
- 6) Datacenter operators can take advantage of the mature O-band component market, offering a wider range of readily available and reliable components.

Fig. 1 provides a summary of the recently reported high-speed demonstrations for O-band IMDD and coherent transmission

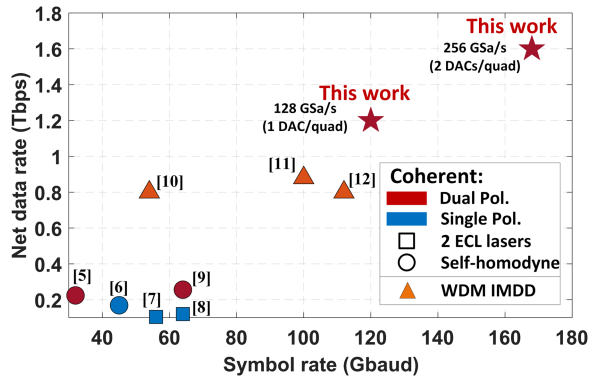


Fig. 1. Review of recent O-band transmission system demonstrations.

systems [5], [6], [7], [8], [9], [10], [11], [12]. Building upon our prior work [13], this study presents the first O-band link operating over 10 km with a net rate exceeding 1 Tbps. The system utilizes a thin-film lithium niobate (TFLN) IQ modulator and two DFB lasers, and compares two generations of digital-to-analog converters (DACs). Specifically, we achieve (a) a net rate of 1.2 Tbps using a single DAC/quadrature (128 GSa/s) at 120 Gbaud DP-64QAM with the  $2.4 \times 10^{-2}$  20% SD-FEC BER threshold, and (b) a net rate of 1.6 Tbps using two interleaved DACs/quadrature (256 GSa/s) at 167 Gbaud DP-64QAM with the  $4 \times 10^{-2}$  25% SD-FEC threshold. We empirically evaluate the transmission performance using the different transmitter configurations and analyze the penalty associated with employing DFB lasers compared to narrow linewidth external cavity lasers (ECL). Additionally, we provide a power consumption comparison of various candidate architectures for 1.6 Tbps transceivers based on the published literature, which further supports our proposal for deploying single-carrier O-band coherent transceivers within datacenters.

The article is organized as follows: Section II provides an overview of the experimental setup configurations. In Section III, we present the achieved transmission performance using the different transmission configurations. Section IV offers a comparison of power consumption among different architectures proposed for 1.6 Tbps operation. Finally, we conclude the work in Section V.

## II. EXPERIMENTAL SETUP AND DIGITAL SIGNAL PROCESSING

Fig. 2 illustrates the experimental setup and the DSP routine employed in the transmission experiment. It includes an amendment made to the figure originally presented in [13]. Starting at the transmitter, we generate a random sequence of QAM symbols using a Mersenne twister. To mitigate pattern-dependent non-linearities in the received signal, we pre-distort the symbols using two lookup tables with a memory length of three for the real (I) and imaginary parts (Q) of the signal. The signal is then filtered using a root-raised cosine (RRC) filter at 2 samples per symbol (sps) and subsequently resampled to match the arbitrary waveform generator (AWG) sampling rate. Additionally, we pre-compensate the frequency response of the transmitter RF

chain (up to the RF probe input) using the digital filters depicted in the inset of Fig. 2. The impact of the pre-emphasis filter is observed on the received RF spectrum as depicted in Fig. 2(b) inset for 120 Gbaud 64QAM signal transmitted using the 128 GSa/s transmitter configuration. Finally, we clip the signal to limit its peak-to-average power ratio (PAPR) to 9 dB and load it onto the AWG.

As shown in Fig. 2, we evaluate the performance using two different transmitter configurations. Configuration (A) consists of a Keysight M8199A AWG (128 GSa/s) without interleaver, followed by an SHF 804 amplifier (22 dB gain and 60 GHz bandwidth), and connected with a 15 cm RF cable (1.85 mm connectors). Configuration (B) utilizes a Keysight M8199B AWG (256 GSa/s) with its internal RF driver, along with a 20 cm RF cable (1.0 mm connectors). The pre-emphasis digital filters shown in Fig. 2(a) inset are generated using a Keysight N1046A-11F 100 GHz digital communication analyzer (DCA), which indicates the inverse of the frequency response of each configuration. The rippled response observed for configuration (A) originates from the RF amplifier and the back reflections caused by cascading connectors. These ripples impose a burden on the receiver equalizer and necessitate the use of a larger number of filter taps to be properly compensated. On the other hand, configuration (B) benefits from the integration of the driver with the DAC, resulting in a smoother response with a slower roll-off. To apply the RF signal to the TFLN IQ modulator, we use a 100 GHz GSG-GSG RF probe. Notably, the I and Q signals on the chip are separated by approximately 625  $\mu\text{m}$  to minimize the RF crosstalk.

The transmitter uses a 1310 nm DFB laser with an output power of 18 dBm, a linewidth ( $\Delta\nu$ ) of 850 kHz measured using the delayed self-homodyne method [14], and a side mode suppression ratio (SMSR) of 49 dB. The single-polarization TFLN IQ modulator has 18 mm coplanar electrodes, resulting in a fiber-to-fiber insertion loss of 10.5 dB, a 6-dB bandwidth of approximately 100 GHz, extinction ratio of 26 dB, and a low-MHz  $V_\pi$  of 1.7 V, as shown in Fig. 3. The low-frequency steep roll-off is a characteristic of traveling-wave modulators, as opposed to the TFLN platform. This phenomenon can be attributed to two primary factors: the RF loss of the electrode, which scales in proportion to  $1/\sqrt{f}$ , and the high sheet resistance of the electrodes at lower frequencies. For dual-polarization (DP) transmission, a DP emulator is employed, consisting of a polarization controller (PC) and a polarization beam splitter (PBS) that split the optical signal into two orthogonal polarizations. One of the polarizations is then delayed by 9.2 ns using a variable optical delay line (VODL) to decorrelate both polarizations during receiver processing. The DP signal is subsequently transmitted over 10 km of standard single-mode fiber (SSMF). To compensate for the lack of transimpedance amplifiers (TIAs) in our receiver, a PDFA is utilized. The received optical power (ROP) is controlled by a variable optical attenuator (VOA) located just before the DP optical hybrid. The other input of the hybrid is connected to another 1310 nm DFB laser, serving as a local oscillator (LO), with an output power of 15 dBm, a linewidth of 400 kHz, and an SMSR of 54 dB, as shown in Fig. 4(a) and (b). The outputs of the hybrid are connected to four

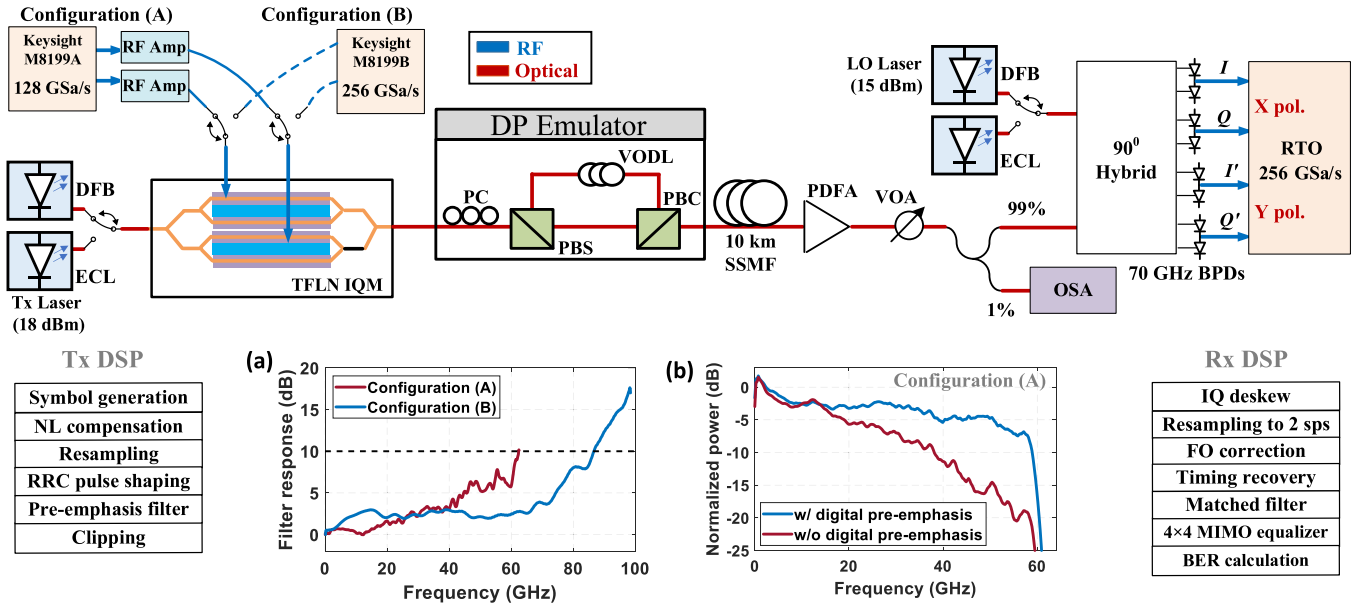


Fig. 2. Experimental setup and the DSP routine employed at the transmitter (Tx) and receiver (Rx) as well as the configuration of DFB or ECL lasers for the carrier and LO sources. The insets show: (a) Digital pre-emphasis filter used with each transmitter configuration (generated from the correction of their frequency response); and (b) received RF spectra of a 120 Gbaud 64QAM signal.

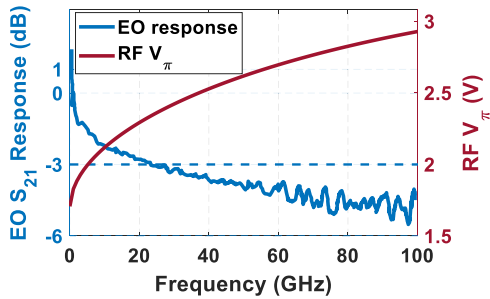


Fig. 3. Electro-optic response of the TFLN modulator (normalized to 1 GHz) and  $RF V_{\pi}$ .

balanced photodiodes with a bandwidth of 70 GHz, which is the main limitation of the system’s bandwidth when configuration (B) is employed.

At the receiver, we initially deskew the signals for each polarization and then correct the frequency offset using the 4th-order method at 2 sps. It is important to note that each DFB laser is equipped with its own thermoelectric cooler (TEC) controller and integrated isolators, and they were very stable in the lab environment. Since we operate in the O-band with minimal chromatic dispersion, we do not require a dedicated DSP block for dispersion compensation. The receiver equalizer consists of a T/2-spaced 81-tap  $4 \times 4$  multiple-input-multiple-output (MIMO) equalizer with real coefficients, interleaved with a first-order phase-locked loop (PLL). We use the same Rx DSP for both transmitter configurations. The use of a real-valued MIMO equalizer provides significant benefits as it independently handles each quadrature of the signal. This approach effectively mitigates power imbalances and any remaining timing skew. Finally, the equalized symbols are mapped back to bits for BER

calculations. As shown in Fig. 2, our experimental setup includes an additional set of ECLs with equivalent output power. These lasers are used to evaluate the penalty associated with employing DFB lasers, as discussed in the next section.

In long-haul C-band coherent transmission systems, the presence of chromatic dispersion introduces significant EEPN, imposing strict requirements on the phase noise of the deployed lasers. Typically, narrow linewidth lasers ( $\Delta\nu < 100$  kHz) are used to mitigate the impact of EEPN. However, operating in the O-band with shorter transmission distances provides the advantage of relaxed laser linewidth requirements, allowing the use of cost-effective DFB lasers. In this work, we utilize commercial-grade DFB lasers with a total linewidth ( $\Delta\nu$ ) of 1.25 MHz. The IEEE P802.3df Ethernet task force is currently exploring coherent solutions for short-reach data center applications, considering laser linewidth up to 3 MHz, with an estimated penalty of 0.4 dB for 1 MHz linewidth [4]. The manageable penalty associated with employing DFB lasers delivers significant cost savings compared to using ECLs. However, it is important to note that the presence of side modes in the laser output can impact the performance of high-symbol rate transmission. The optical spectra for 120 Gbaud 64QAM (configuration (A)) and 180 Gbaud 64QAM (configuration (B)) are illustrated in Fig. 4(c). The highlighted spectral broadening is attributed to the non-linearity introduced from the TFLN modulator. Yet, we observe the beating of the LO laser with the first side mode from the Tx laser, which is only 47 GHz away from the main mode, on the real-time oscilloscope (RTO) in the absence of the signal. This beating will impact the transmission performance and it is better if there is no overlap between the side modes and the signal spectrum. Hence, the side mode suppression ratio (SMSR) and spectral separation between modes, alongside the linewidth, are important parameters to consider when evaluating

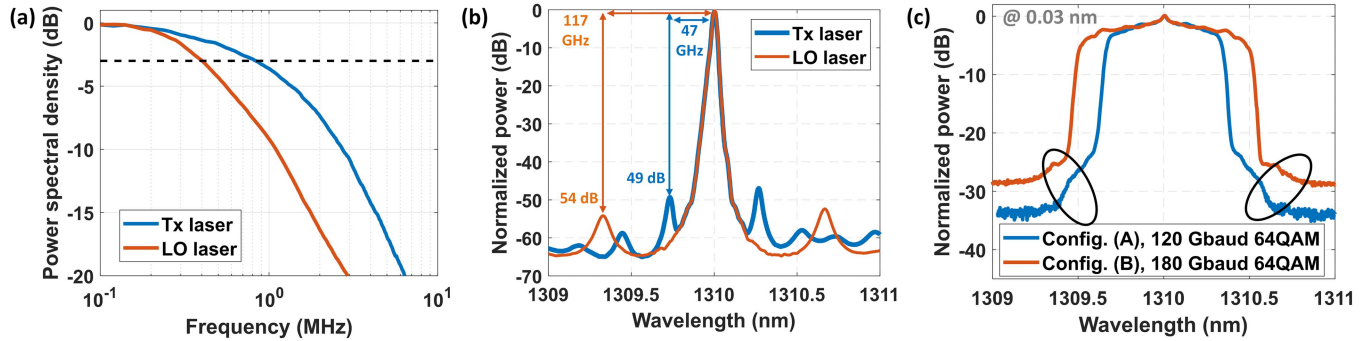


Fig. 4. (a) Power spectral density of the two DFB lasers based on the self-homodyne measurement; (b) optical spectra of each DFB laser without signal; and (c) optical spectra at the input of optical hybrid of a 120 Gbaud and 180 Gbaud DP-64QAM.

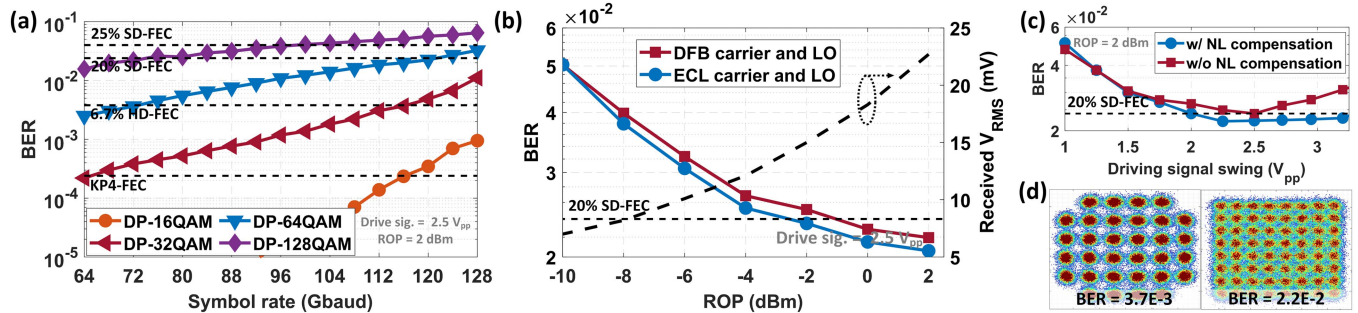


Fig. 5. (a) BER versus the symbol rate after 10 km of SSMF using DFB lasers for both the carrier and the LO. (b) BER sensitivity to the ROP as a function of laser type and the corresponding received RMS level. (c) BER of a 120 Gbaud DP-64QAM signal versus the IQM driving swing with and without nonlinear compensation. (d) Received constellations of one polarization of a 120 Gbaud DP-64QAM and a DP-32QAM signal.

TABLE I  
SUMMARY OF NET BITRATE ACHIEVED AFTER 10 KM TRANSMISSION USING DFB LASERS

		Keysight M8199A (128 GSa/s)		Keysight M8199B (256 GSa/s)		
		1 DAC/quadrature		2 DACs/quadrature		
BER threshold	FEC overhead	Modulation format	Net bitrate (Tbps)	Modulation format	Net bitrate (Tbps)	Gain (%)
$2.4 \times 10^{-4}$	5%	116 Gbaud DP-16QAM	0.88	148 Gbaud DP-16QAM	1.12	27
$3.8 \times 10^{-3}$	6.7%	116 Gbaud DP-32QAM	1.09	144 Gbaud DP-32QAM	1.35	24
$2.4 \times 10^{-2}$	20%	120 Gbaud DP-64QAM	1.2	180 Gbaud DP-32QAM	1.5	25
$4 \times 10^{-2}$	25%	128 Gbaud DP-64QAM	1.23	167 Gbaud DP-64QAM	1.6	30

the suitability of DFB lasers for these systems. The disparity in the observed ASE noise level depicted in Fig. 4(c) can be attributed to the difference in driving voltage swing at 120 and 180 Gbaud, resulting from the digital pre-emphasis filtering. This leads to higher modulation loss for the 180 Gbaud signal, resulting in a lower input power into the PDFA and consequently lower optical SNR.

### III. TRANSMISSION EXPERIMENT RESULTS

#### A. Configuration A: (128 GSa/s)

Here, we present the achieved transmission performance using configuration (A) of the transmitter, consisting of a 128 GSa/s DAC followed by a 22 dB RF amplifier. Fig. 5(a) plots the BER versus symbol rate for different QAM formats after

10 km transmission. With this configuration, we successfully transmit 120 Gbaud DP-64QAM, achieving a BER below the  $2.4 \times 10^{-2}$  20% overhead SF-FEC threshold, corresponding to a net capacity of 1.2 Tbps. A summary of the performance at the different FEC thresholds is provided in Table I. In this configuration, the primary bandwidth limitation stems from the transmitter.

Fig. 5(b) demonstrates the BER sensitivity to the ROP at the input of the optical hybrid for 120 Gbaud DP-64QAM. We compare the achieved BER using the DFB laser set with the ECL set to evaluate the penalty resulting from the linewidth (phase noise) difference. The transmitter ECL has 100 kHz linewidth, while the LO laser has 500 kHz linewidth; thus, the total linewidth of this configuration is 0.6 MHz compared to 1.25 MHz for the DFB set. Both sets exhibit similar behavior,

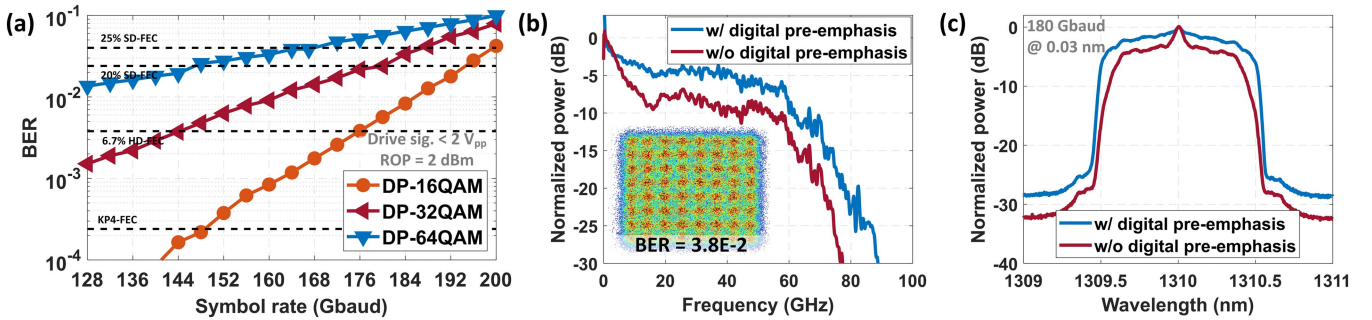


Fig. 6. (a) BER versus the symbol rate after 10 km of SSMF using DFB lasers for both the carrier and the LO. (b) Received RF spectra of 180 Gbaud 32QAM with and without digital pre-emphasis, with the inset showing the constellation of the X-pol of 167 Gbaud DP-64QAM. (c) Optical spectra of 180 Gbaud DP-32QAM signal after fiber transmission.

with the BER limited by the analog-to-digital converter (ADC) noise below  $-4$  dBm. However, as the ROP increases, the BER approaches a floor due to the dominance of PDFSA ASE noise. At the 20% SD-FEC threshold, the gain of using ECLs is less than 1 dB, aligning with industry estimates and supporting the adoption of high-quality DFB lasers in short-reach coherent transponders [4].

Fig. 5(c) shows the BER sensitivity to the driving voltage swing at the input of the RF probe, with and without non-linear pre-compensation. The observed optimal driving swing is  $2.5 V_{pp}$ , which is the 1 dB compression point of the SHF 804 RF amplifier. Owing to the low  $V_{\pi}$  (half-wave voltage) of TFLN, there is no need to drive the amplifier beyond its 1 dB point, resulting in improved linearity of the transmitted signal. We observe a marginal gain when employing non-linear pre-compensation, as demonstrated in the constellations presented in Fig. 5(d). The constellations for the X-pol of 120 Gbaud DP-64QAM and DP-32QAM appear linear and symmetric, indicating that the real-valued MIMO effectively mitigates any power imbalances between the I and Q quadratures.

### B. Configuration B (256 GSa/s)

To explore higher capacity limits and assess the advantages of next-generation DACs, we present the transmission performance achieved using configuration (B) of the transmitter. This configuration utilizes a 256 GSa/s DAC with a 6 dB bandwidth of 85 GHz and an output single-ended swing of  $2.5 V_{pp}$ . In this setup, we only use DFB lasers. Fig. 6(a) and Table I provide a summary of the BER performance for various QAM formats. We successfully transmit 167 Gbaud DP-64QAM over 10 km, achieving a BER below the  $4 \times 10^{-2}$  SD-FEC threshold. This demonstrates the first O-band transmission system capable of supporting a net capacity of 1.6 Tbps over a single fiber. Additionally, we transmit 180 Gbaud DP-32QAM below the  $2.4 \times 10^{-2}$  SD-FEC threshold, corresponding to net capacity 1.5 Tbps. This represents a 25% performance gain compared to configuration (A) at the same FEC threshold. The last column of Table I reports the net transmission rate gain achieved when this configuration is utilized compared to configuration (A) at the different FEC thresholds. It is fair to say that  $\sim 25\%$  improvement is observed for this configuration. However, the actual gain

is even higher, as configuration (B) is limited by the 70 GHz balanced photodiodes (BPDs).

Fig. 6(b) plots the received RF spectra with and without digital pre-emphasis for the 180 Gbaud 32QAM signal. This work solely relies on electronic equalization techniques, similar to those employed in practical networks, without the inclusion of optical shaping or optical equalization methods. The pre-emphasis filter compensates for the frequency response of the transmitter RF chain. Therefore, the uncompensated chain includes the 100 GHz RF probe, the TFLN modulator, the 70 GHz BPDs, and the 100 GHz ADCs. A  $\sim 20$  dB drop at 80 GHz is observed, primarily attributed to the limited bandwidth of the BPDs. In alignment with this observation, the optical spectra of the 180 Gbaud DP-32QAM signals depicted in Fig. 6(c) exhibit a flatter response up to the signal bandwidth. This suggests that the TFLN IQ modulator has the potential to support higher data rates if higher bandwidth photodiodes are used in the system.

## IV. POWER CONSUMPTION ANALYSIS

This section presents an analysis of the power consumption envelope (the DSP and optical engines; not the total power) for the key candidate architectures capable of achieving 1.6 Tbps transmission. The system architectures considered are as follows:

- 1)  $8\lambda \times 200$  Gbps WDM IMDD: This configuration utilizes silicon photonic (SiP) modulators, which are commonly utilized at these data rates [15].
- 2)  $4\lambda \times 400$  Gbps WDM IMDD: Compared to the  $8 \times 200$  Gbps configuration, this configuration requires higher bandwidth modulators. In our analysis, we assume the use of TFLN technology to meet these requirements [16].
- 3)  $2\lambda \times 800$  Gbps WDM coherent transmission: This configuration utilizes SiP IQ modulators, as it is equivalent to 200 Gbps per quadrature [17].
- 4)  $1\lambda \times 1.6$  Tbps single-carrier coherent transmission: Based on the transmission performance demonstrated in the previous section, we assume it is realized using TFLN platform [13].

Each of these configurations presents its own set of technical challenges and hardware requirements. The power consumption analysis aims to provide insights into the relative energy

efficiency of these options, allowing for a more comprehensive evaluation of their performance. Considering a set of assumptions outlined in the appendix, our analysis is based on publicly reported data from the literature on the power consumption of discrete components. However, it is important to note that power consumption can vary among different vendors due to variations in product features and characteristics. Therefore, we aim to provide a fair and objective comparison between the different architectures, without referring to a specific vendor or product.

As detailed in the appendix, Fig. 7(a) provides the breakdown of power consumption for the various architectures, along with the overall consumption given in Fig. 7(b). It is worth noting that this is not the total power of the entire pluggable optical transceiver module. This is because we are specifically referring to the power consumed by the optical and RF components and not taking into account other components present in the module, which have similar power requirements regardless of the architecture. These additional components include the central processing unit (CPU), Ethernet framer and mapper, and the microcontroller used for interfacing. Furthermore, the analysis presented here does not consider the finite DC/DC power conversion efficiency as it does not depend on the transceiver architecture.

In all four architectures, the main consumption comes from the DSP and DAC/ADCs, with the  $4\lambda \times 400$  Gbps IMDD proposal exhibiting the lowest power consumption in this respect. This same architecture is, notwithstanding, the least efficient in terms of the power required to operate the TECs, resulting in a total power consumption of 14.5 W. By operating at a lower symbol rate and doubling the optical channel count, it becomes possible to mitigate the impairments caused by chromatic dispersion and eliminate the requirement for precise wavelength control using TECs. As a result, the  $8\lambda \times 200$  Gbps IMDD architecture becomes as power-efficient as the  $4\lambda \times 400$  Gbps architecture. Considering the implementation challenges associated with the  $4\lambda \times 400$  Gbps IMDD architecture (see Table II), the  $8\lambda \times 200$  Gbps architecture seems to be a more sensible solution within the IMDD realm. The  $2\lambda \times 800$  Gbps coherent architecture consumes 40% more power compared to the single carrier 1.6 Tbps architecture. This increased power consumption can be attributed to the higher driving voltage requirements for SiP technology and the doubling of hardware components, as demonstrated in Table III. On the other hand, our analysis reveals that the  $1\lambda \times 1.6$  Tbps TFLN-based coherent solution exhibits the lowest power consumption, requiring less than 14 W. This low power consumption envelope is attributed to the simpler architecture and inherent disparities between SiP and TFLN platforms, which makes it highly competitive, even when compared to IMDD architectures. Furthermore, this architecture has the lowest hardware requirements, as indicated in Table III, which directly translates to a smaller transceiver footprint. The low power consumption and small footprint suggest that the  $1\lambda \times 1.6$  Tbps TFLN-based coherent architecture can be realized with the current state-of-the-art small form-factor pluggable (SSFP) modules. This result, together with its feasibility (demonstrated in Section III), strongly supports our proposition to consider O-band TFLN-based single-carrier coherent transmission as the

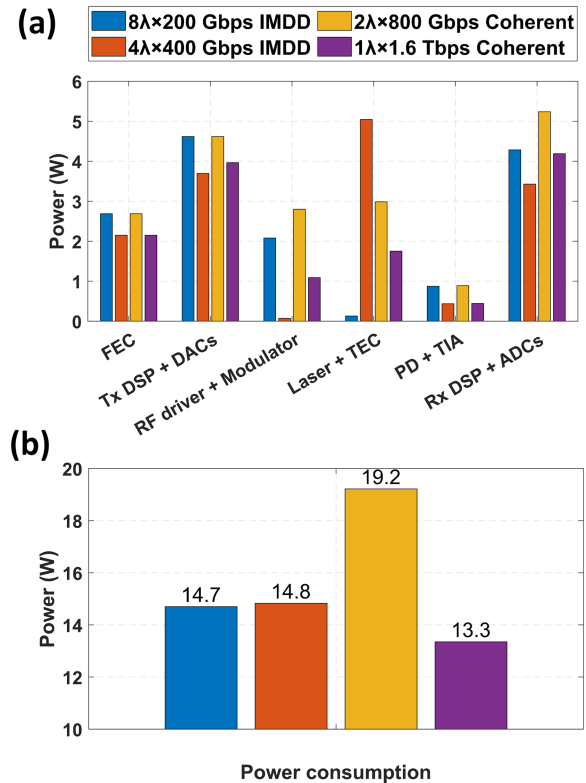


Fig. 7. (a) Power consumption breakdown and (b) calculated total power (DSP and optical engines) for the candidate architectures for 1.6 Tbps operation.

main contender for the deployment of next-generation 1.6 Tbps intra-datacenter interconnects.

## V. CONCLUSION

This work presents the first demonstration of a single-carrier O-band coherent transmission system operating with a net capacity of 1.6 Tbps over 10 km of SSMF, enabled by next-generation DACs and the TFLN platform. Furthermore, we demonstrate the feasibility of employing cost-effective DFB lasers in such systems, incurring a manageable penalty of less than 1 dB with respect to the use of narrow-linewidth lasers. These experimental results, together with a comprehensive power consumption estimation based on the public literature, showcase the advantages of this high performance and power efficient solution when compared to other key candidate architectures that have been envisaged for the 1.6 Tbps Ethernet implementation. Therefore, our research results support the adoption of the O-band single-carrier coherent solution for next-generation intra-datacenter interconnects.

## APPENDIX

In this appendix, we provide a detailed explanation of the assumptions and calculations used in the power consumption comparison. The following assumptions apply to all the configurations:

TABLE II  
THE DETAILED CALCULATIONS AND ASSUMPTIONS USED IN THE POWER CONSUMPTION ANALYSIS

Arch.	8λ×200 Gbps WDM IMDD	4λ×400 Gbps WDM IMDD	2λ×800 Gbps WDM coherent transmission	1λ×1.6 Tbps single-carrier coherent transmission
Format / Spect. eff.	120 Gbaud PAM4 (1.6×10 <sup>9</sup> bit/s/Hz)	192 Gbaud PAM6 (2×10 <sup>9</sup> bit/s/Hz)	120 Gbaud DP-16QAM (6.5×10 <sup>9</sup> bit/s/Hz)	192 Gbaud DP-32QAM (8.2×10 <sup>9</sup> bit/s/Hz)
	<ul style="list-style-type: none"> <li>The assumed symbol rate and modulation formats leaves 20% margin for the FEC and switching overheads</li> </ul>			
FEC	<ul style="list-style-type: none"> <li>It is envisioned that a stronger FEC like the C-FEC (14.8% overhead) will be used in the next-generation applications, which consumes 420 mW (7 nm process node) for 400 Gbps transmitters [18]. This corresponds to 2×420 mW for 60 Gbaud DP-16QAM, to account for both the encoder and decoder.</li> <li>We assume that the power consumption of the FEC (digital circuit) module scales linearly with symbol rate.</li> <li>We assume a 20% power reduction when scaling from 7 nm to 5 nm process node.</li> </ul>			
	420×(8/4)×(120/60)×0.8×2	420×(4/4)×(192/60)×0.8×2	420×(8/4)×(120/60)×0.8×2	420×(4/4)×(192/60)×0.8×2
	<b>P<sub>FEC</sub> = 2.67 W</b>	<b>P<sub>FEC</sub> = 2.15 W</b>	<b>P<sub>FEC</sub> = 2.67 W</b>	<b>P<sub>FEC</sub> = 2.15 W</b>
Tx DSP including DAC	<ul style="list-style-type: none"> <li>Ref. [19] demonstrated a CMOS (10 nm process node) DAC operating at 112 GSa/s with 8-tap feed-forward equalizer (FFE). That DAC has an output swing of 1 V<sub>pp</sub> and consumes 432 mW.</li> <li>We assume the DAC power consumption scales linearly with the sampling rate as in [20].</li> <li>For calculations, we assume that the overall power consumption of this transmitter to be 600 mW, where the digital DSP blocks consumes 170 mW, and the analog part consumes the remaining 430 mW.</li> <li>Then we scale only the digital part by 20%×20% for moving from 10 nm to 5 nm process node.</li> <li>This is power consumption per lane or quadrature; thus, we scale it accordingly. The transmitter DSP for IMDD and coherent transmission are very similar; hence, we use the same calculations for both schemes.</li> </ul>			
	(170×0.8×0.8+430)×8×(120/112)	(170×0.8×0.8+430)×4×(192/112)	(170×0.8×0.8+430)×8×(120/112)	(170×0.8×0.8+430)×4×(192/112)
	<b>P<sub>Tx_ASIC</sub> = 4.618 W</b>	<b>P<sub>Tx_ASIC</sub> = 3.694 W</b>	<b>P<sub>Tx_ASIC</sub> = 4.618 W</b>	<b>P<sub>Tx_ASIC</sub> = 3.694 W</b>
RF Driver	<ul style="list-style-type: none"> <li>For TFLN, the typical V<sub>π</sub> of the MZM is 1.5 V; thus, operating without RF driver is feasible [21]. Yet, driving the TFLN IQM requires ~ 2 V<sub>pp</sub> and an RF driver with 6-10 dB gain.</li> <li>The SiP MZMs has a typical V<sub>π</sub> of 6 V [22], which requires 10-16 dB RF driver. For coherent transmission, we assume a 20 dB gain RF driver.</li> <li>Ref. [23] reported a 4-channel linear driver with 48 GHz bandwidth and 13-22.5 dB tuneable gain, which consumes 225 mW per channel and is realized with a 65 nm CMOS process.</li> </ul>			
	225×8	-	225×8	225×4
	<b>P<sub>Tx_driver</sub> = 1.8 W</b>	<b>P<sub>Tx_driver</sub> = 0 W</b>	<b>P<sub>Tx_driver</sub> = 1.8 W</b>	<b>P<sub>Tx_driver</sub> = 0.9 W</b>
Laser	<ul style="list-style-type: none"> <li>Following [2], we calculate the optical power budget for each configuration and offset it relative to each other.</li> <li>The power consumption of a laser diode is given by <math>P_{LD} = V_{LD,f} I_{LD,driv}</math>; and <math>I_{LD,driv} = P_{LD,opt}/\gamma_{LD} + I_{LD,th}</math>. Where <math>V_{LD,f}</math> is the diode bias voltage, <math>I_{LD,driv}</math> is the diode current, <math>P_{LD,opt}</math> is the optical power of the laser, <math>\gamma_{LD}</math> is the slope efficiency, and <math>I_{LD,th}</math> is the threshold current.</li> <li>These parameters differ among vendors. A typical set of values are <math>V_{LD,f} = 1.6 V</math>, <math>I_{LD,th} = 15 mA</math>, and <math>\gamma_{LD} = 0.29 mW/mA</math> [24].</li> </ul>			
	Link budget: <ul style="list-style-type: none"> <li>SiP chip IL = 8.5 dB (4 dB coupling and 4.5 dB MZM IL)</li> <li>Modulation loss = 3 dB</li> <li>Optical Mux/Demux IL = 4 dB</li> <li>10 km fiber = 3.5 dB</li> <li>8-channel implementation = -9 dB (It is a gain in the link budget as we calculate the power required per laser)</li> </ul>	Link budget: <ul style="list-style-type: none"> <li>TFLN chip IL = 6 dB (4 dB coupling and 2 dB MZM IL)</li> <li>Modulation loss = 3 dB</li> <li>Optical Mux/Demux IL = 4 dB</li> <li>10 km fiber = 3.5 dB</li> <li>Rx chip IL = 2 dB</li> <li>The OSNR penalty (Relative to 120 Gbaud PAM4) = 8.2 dB</li> <li>4-channel implementation = -6 dB</li> </ul>	Link budget: <ul style="list-style-type: none"> <li>SiP chip IL = 12 dB (4 dB coupling, 6 dB DP IQM, and 2 dB for the optical hybrid)</li> <li>Modulation loss = 12 dB (because of the high V<sub>π</sub>)</li> <li>Optical Mux/Demux IL = 4 dB</li> <li>10 km fiber = 3.5 dB</li> <li>2-channel implementation = -3 dB</li> </ul>	Link budget: <ul style="list-style-type: none"> <li>TFLN chip IL = 7.5 dB (4 dB coupling and 3.5 dB DP IQM)</li> <li>Modulation loss = 8 dB (for linear performance)</li> <li>10 km fiber = 3.5 dB</li> <li>Rx chip IL = 4 dB (including the hybrid)</li> <li>The OSNR penalty (Relative to 120 Gbaud PAM4) = 8.2 dB</li> </ul>
	Total link budget = 10 dB	Total link budget = 20.7 dB	Total link budget = 28.5 dB	Total link budget = 31.2 dB
	<ul style="list-style-type: none"> <li>Based on the total link budget, we assume that the 1×1.6 Tbps configuration will use a 20 dBm laser source and scale the other configurations according to the number of lasers needed and their projected optical power.</li> <li>In coherent transceivers, a single laser is split to act as a Tx source and LO for bidirectional transmission. Thus, the calculated laser power is total power after combining both sources.</li> </ul>			
	Laser power assumed = -1.2 dBm $P_{LD} = 16.25 mW$	Laser power assumed = 9.5 dBm $P_{LD} = 61 mW$	Laser power assumed = 17.3 dBm $P_{LD} = 307.5 mW$	Laser power assumed = 20 dBm $P_{LD} = 575 mW$
	<b>P<sub>laser</sub> = 0.01625×8 = 0.13 W</b>	<b>P<sub>laser</sub> = 0.061×4 = 0.244 W</b>	<b>P<sub>laser</sub> = 0.307×2 = 0.615 W</b>	<b>P<sub>laser</sub> = 0.575 W</b>
TEC controller	<ul style="list-style-type: none"> <li>IMDD systems do not necessarily require the use of a thermoelectric cooler (TEC) when a wide-spacing WDM grid is adopted. However, the edge channels may experience severe chromatic dispersion, especially in the 4×400 Gbps configuration. Thus, the 4×400 Gbps requires smaller spacing in the WDM grid and more accurate control over their wavelengths. Accordingly, we assume that the 4×400 Gbps IMDD solution employs a TEC similar to coherent architectures.</li> <li>Based on [25], the TEC consumes ~ 1200 mW.</li> </ul>			
	-	1200×4	1200×2	1200×1
	<b>P<sub>TEC</sub> = 0 W</b>	<b>P<sub>TEC</sub> = 4.8 W</b>	<b>P<sub>TEC</sub> = 2.4 W</b>	<b>P<sub>TEC</sub> = 1.2 W</b>

TABLE II  
CONTINUED.

Modulator	<ul style="list-style-type: none"> <li>We assume that a series push pull (SPP) MZM / IQM is used, and the driving swing depends on the architecture and modulator platform.</li> <li>For IMDD, the power consumption in the modulator is given by <math>P_{modulator} = P_{MZM} + P_{\pi,TPS}/2</math>, where <math>P_{MZM}</math> is the power consumed in the RF termination and equals <math>P_{MZM} = V_{rms}^2/R</math> with R typically 50 <math>\Omega</math>. <math>P_{\pi,TPS}</math> is the power consumed by the thermal phase shifter to induce a phase-shift of <math>\pi</math>.</li> <li>For coherent transmission, there are 4 MZMs in the DP IQM. Thus, it consumes <math>P_{total} = 4 \times P_{MZM} + 5 \times P_{\pi,TPS}</math></li> <li><math>P_{\pi,TPS} = 30</math> mW</li> </ul>			
	• For SiP IMDD [22], $V_{rms} = 1$ V ( $1^2/50 + 0.015$ ) $\times 8$	• For TFLN IMDD [21], $V_{rms} =$ 0.35 V ( $0.35^2/50 + 0.015$ ) $\times 4$	• For SiP coherent [22], $V_{rms} =$ 2.12 V ( $4 \times (2.12^2/50) + 5 \times 0.03$ ) $\times 2$	• For TFLN coherent [13], $V_{rms} =$ 0.7 V ( $4 \times (0.7^2/50) + 5 \times 0.03$ )
	<b><math>P_{modulator} = 0.28</math> W</b>	<b><math>P_{modulator} = 0.07</math> W</b>	<b><math>P_{modulator} = 1</math> W</b>	<b><math>P_{modulator} = 0.19</math> W</b>
	<ul style="list-style-type: none"> <li>PDs consume negligible power under reverse bias, typically 2 mW per PD.</li> </ul>			
PD	<b><math>P_{PD} = 0.016</math> W</b>	<b><math>P_{PD} = 0.008</math> W</b>	<b><math>P_{PD} = 0.032</math> W</b>	<b><math>P_{PD} = 0.016</math> W</b>
TIA	<ul style="list-style-type: none"> <li>In [26], the authors demonstrated a 60 GHz single-ended TIA that consumes 107 mW and is realized with 28 nm CMOS process.</li> <li>The TIA power consumption does not depend on the architecture. It depends on the receiver sensitivity and required gain, which are assumed to be the same for the different configurations.</li> </ul>			
	(107) $\times 8$	(107) $\times 4$	(107) $\times 8$	(107) $\times 4$
	<b><math>P_{TIA} = 0.856</math> W</b>	<b><math>P_{TIA} = 0.428</math> W</b>	<b><math>P_{TIA} = 0.856</math> W</b>	<b><math>P_{TIA} = 0.428</math> W</b>
Rx DSP including ADC	<ul style="list-style-type: none"> <li>The receiver DSP for IMDD and coherent transmission are different. Based on [2], the power consumption of the coherent DSP is 1.6<math>\times</math> (60% higher) that of IMDD at the same symbol rate. This included the power consumption of the chromatic dispersion compensation module, which is actually not needed since we operate in the O-band.</li> <li>Ref. [27] reported a CMOS (5 nm process node) SerDes receiver, which is composed of a 112 GSa/s ADC and 16 tap FFE. The analog circuit consumes 315 mW and we assume that the digital part consumes additional 185 mW.</li> <li>We assume that the power consumption of the ADC and DSP scales linearly with symbol rate.</li> </ul>			
	500 $\times$ (120/112) $\times 8$	500 $\times$ (192/112) $\times 4$	(185 $\times 1.6 + 315$ ) $\times$ (120/112) $\times 8$	(185 $\times 1.6 + 315$ ) $\times$ (192/112) $\times 4$
	<b><math>P_{Rx\_ASIC} = 4.285</math> W</b>	<b><math>P_{Rx\_ASIC} = 3.428</math> W</b>	<b><math>P_{Rx\_ASIC} = 5.237</math> W</b>	<b><math>P_{Rx\_ASIC} = 4.19</math> W</b>
Total power	<ul style="list-style-type: none"> <li>The calculated power is not the power of the entire optical transceiver pluggable module, as we do not include the central processing unit (CPU) power consumption, Ethernet framer and mapper, and the microcontroller for interfacing. In addition, we did not include the DC/DC power conversion efficiency. The power consumption of these units is almost independent of the optical transceiver architecture; hence, we exclude it from the discussion.</li> <li>There should be some resource sharing between modules if multiples components are integrated together; however, this value is hard to estimate from the public literature. Hence, resource sharing is not accounted for in the analysis.</li> <li>It is worth noting that this is a best-case (conservative) estimate, which can not be directly compared with what vendors report.</li> </ul>			
	<b><math>P_{total} = 14.7</math> W</b>	<b><math>P_{total} = 14.83</math> W</b>	<b><math>P_{total} = 19.22</math> W</b>	<b><math>P_{total} = 13.35</math> W</b>
Technical challenges	<ul style="list-style-type: none"> <li>Although this architecture employs a mature 200 Gbps per lane transceiver, the technical challenges reside in the integration and packaging of 8 transceivers in a small form factor pluggable module.</li> <li>Another concern is its low spectral efficiency.</li> </ul>	<ul style="list-style-type: none"> <li>Technically, this is the most challenging architecture to realize. Employing the conventional CWDM4 grid is not feasible because of the chromatic dispersion-induced power fading at the edge channels. Using a narrower WDM grid mitigates chromatic dispersion, but it introduces significant fiber non-linearities and four-wave mixing (FWM).</li> <li>The transfer function of a dispersive IMDD system is given by: <math>H(\omega) = \left  \cos\left(\frac{\beta_2 \omega^2 L}{2}\right) \right </math>, which results in a spectral dip at <math>f = \sqrt{\frac{1}{4\pi \beta_2 L}}</math>. Thus, transmitting high symbol rate WDM IMDD signals is prohibitive.</li> <li>In addition, it requires precise control of lasers' wavelengths (increase in cost) and specially designed Mux/Demux if a narrower WDM grid is utilized.</li> <li>The footprint of TFLN MZMs is large (integration challenge)</li> </ul>	<ul style="list-style-type: none"> <li>800 Gbps SiP coherent transceivers exist on a commercial scale, the challenge is to integrate two transceivers in the same small form-factor pluggable module.</li> <li>The other challenge is to reduce the high power consumption envelope for this architecture.</li> <li>The fan-out granularity is limited to 800 Gbps.</li> </ul>	<ul style="list-style-type: none"> <li>The TFLN IQM has large footprint, which poses some integration and packaging challenges.</li> <li>It requires high power laser sources.</li> <li>The fan-out granularity is limited to 1.6 Tbps.</li> </ul>



TABLE III  
THE HARDWARE REQUIREMENTS FOR THE DIFFERENT ARCHITECTURES

Architecture	8λ×200 Gbps WDM IMDD	4λ×400 Gbps WDM IMDD	2λ×800 Gbps WDM coherent transmission	1λ×1.6 Tbps single-carrier coherent transmission
Lasers	8	4	2	1
TECs	-	4	2	1
MZMs	8	4	8 (2 DP IQMs)	4 (1 DP IQMs)
Optical Mux/Demux	1	1	1	-
RF Drivers	8	-	8	4
DACs	8	4	8	4
ADCs	8	4	8	4
PDs	8	4	8	4
TIAs	8	4	8	4
ASIC DSP	1	1	1	1
Optical hybrid	-	-	2	1
Total count (#) of components	58	30	56	28

- 1) Operating Band and Distance: We assume that all configurations operate in the O-band and are evaluated for a transmission distance of 10 km.
- 2) DSP Engine: The DSP engine is assumed to support a fixed modulation format and symbol rate without employing geometric or probabilistic constellation shaping techniques.
- 3) RF Componentry Bandwidth: It is assumed that the performance of the RF componentry, such as RF drivers and TIAs, does not limit the overall system performance and evolves naturally with advancements in technology.
- 4) ASIC Process Node: The DSP engine is realized using the 5 nm process node.

These assumptions serve as the basis for the power consumption analysis and facilitate a fair comparison among the different architectures. The details of the calculations used to generate Fig. 7 are given in Table II.

#### ACKNOWLEDGMENT

The authors would like to thank HyperLight for their support on the TFLN modulator and Santec for providing the high-power ECL. R.G.C. is grateful to Dir. Gral. de Asuntos del Personal Académico, UNAM for supporting him through a sabbatical scholarship, and PAPIIT project IN103122.

#### REFERENCES

- [1] "800G pluggable MSA," 2019. Accessed: May 13, 2023. [Online]. Available: <https://www.800gmsa.com>
- [2] J. Cheng, C. Xie, Y. Chen, X. Chen, M. Tang, and S. Fu, "Comparison of coherent and IMDD transceivers for intra datacenter optical interconnects," in *Proc. IEEE Opt. Fiber Commun. Conf.*, 2019, pp. 1–3.
- [3] C. Lam, X. Zhou, and H. Liu, "Coherent-lite for beyond 400GbE," IEEE 802.3 Beyond 400 Gb/s Ethernet Study Group Meeting, 2021. Accessed: May 18, 2023. [Online]. Available: [https://www.ieee802.org/3/B400G/public/21\\_07/lam\\_b400g\\_01a\\_210720.pdf](https://www.ieee802.org/3/B400G/public/21_07/lam_b400g_01a_210720.pdf)
- [4] J. Harley, D. Meghan, S. O. Gharan, and E. Maniloff, "Coherent Laser specifications and control for 800G 10km application," IEEE P802.df 400 Gb/s and 800 Gb/s Ethernet Task Force Meeting, 2022. Accessed: May 15, 2023. [Online]. Available: [https://www.ieee802.org/3/df/public/22\\_11/maniloff\\_3df\\_01\\_2211.pdf](https://www.ieee802.org/3/df/public/22_11/maniloff_3df_01_2211.pdf)
- [5] C. Doerr et al., "O, E, S, C, and L band silicon photonics coherent modulator/receiver," in *Proc. IEEE Opt. Fiber Commun. Conf. Exhib.*, 2016, pp. 1–3.
- [6] A. Samani et al., "180 Gb/s single carrier single polarization 16-QAM transmission using an O-band silicon photonic IQM," *Opt. Exp.*, vol. 27, no. 10, pp. 14447–14456, 2019.
- [7] P. M. Seiler et al., "56 GBaud O-band transmission using a photonic BiCMOS coherent receiver," in *Proc. IEEE Eur. Conf. Opt. Commun.*, 2020, pp. 1–4.
- [8] P. M. Seiler et al., "Multiband silicon photonic ePIC coherent receiver for 64 GBd QPSK," *J. Lightw. Technol.*, vol. 40, no. 10, pp. 3331–3337, May 2022.
- [9] A. Maharry et al., "First demonstration of an O-band coherent link for intra-data center applications," in *Proc. IEEE Eur. Conf. Opt. Commun.*, 2022, pp. 1–4.
- [10] L. Chorchos and J. P. Turkiewicz, "O-band 8 × 100 G data transmission with 240 GHz channel spacing," *IEEE Commun. Lett.*, vol. 23, no. 12, pp. 2288–2291, Dec. 2019.
- [11] K. Wang, J. Zhang, M. Zhao, W. Zhou, L. Zhao, and J. Yu, "High-speed PS-PAM8 transmission in a four-lane IM/DD system using SOA at O-band for 800G DCI," *IEEE Photon. Technol. Lett.*, vol. 32, no. 6, pp. 293–296, Mar. 2020.
- [12] H. Taniguchi, S. Yamamoto, A. Masuda, Y. Kisaka, and S. Kanazawa, "800-Gbps PAM-4 2-km transmission using 4-λ LAN-WDMTOSA with MLSE based on deep neural network," in *Proc. Opt. Fiber Commun. Conf.*, 2022, Paper Th2A. 25.
- [13] E. Berikaa et al., "Net 1.6 Tbps O-band coherent transmission over 10 km using a TFLN IQM and DFB lasers for carrier and LO," in *Proc. Opt. Fiber Commun. Conf.*, 2023, Paper Th4B. 1.
- [14] H. Ludvigsen, M. Tossavainen, and M. Kaivola, "Laser linewidth measurements using self-homodyne detection with short delay," *Opt. Commun.*, vol. 155, no. 1/3, pp. 180–186, 1998.
- [15] P. Xia et al., "8 × 250 Gbit/s PAM4 transmission over 1 km single mode fiber with an all-silicon LAN WDM transmitter," in *Proc. IEEE Opt. Fiber Commun. Conf.*, 2023, pp. 1–3.
- [16] E. Berikaa, M. S. Alam, and D. V. Plant, "Net 400-Gbps/λ IMDD transmission using a single-DAC DSP-free transmitter and a thin-film lithium niobate MZM," *Opt. Lett.*, vol. 47, no. 23, pp. 6273–6276, 2022.
- [17] E. Berikaa, M. S. Alam, A. Samani, S. Lessard, and D. V. Plant, "Net 1 Tbps/λ transmission over 80 km of SSMF using a single segment SiP IQM with all-electronic equalization," in *Proc. Opt. Fiber Commun. Conf.*, 2022, Paper Th4A. 5.
- [18] I. Lyubomirsky, J. Riani, B. Smith, S. Bhoja, and R. Baca, "Baseline proposal for 400G/80km," 2018. Accessed: May 20, 2023. [Online]. Available: [https://www.ieee802.org/3/cn/public/18\\_11/lyubomirsky\\_3cn\\_02a\\_1118.pdf](https://www.ieee802.org/3/cn/public/18_11/lyubomirsky_3cn_02a_1118.pdf)

- [19] J. Kim et al., "8.1 a 224Gb/s DAC-based PAM-4 transmitter with 8-tap FFE in 10nm CMOS," in *Proc. IEEE Int. Solid-State Circuits Conf.*, 2021, pp. 126–128.
- [20] Z. Jiang, "High data rate DMT SERDES design," Ph.D. dissertation, Carleton Univ., Ottawa, ON, Canada, 2022.
- [21] E. Berikaa, M. S. Alam, and D. V. Plant, "Beyond 300 Gbps short-reach links using TFLN MZMs With 500 mV pp and linear equalization," *IEEE Photon. Technol. Lett.*, vol. 35, no. 3, pp. 140–143, Feb. 2023.
- [22] C. Lam, X. Zhou, and H. Liu, "200G per lane for beyond 400GbE," in *Proc. IEEE 802.3 NEA Meeting*, 2020, pp. 1–20.
- [23] T. Jyo, M. Nagatani, J. Ozaki, M. Ishikawa, and H. Nosaka, "12.3 A 48GHz BW 225mW/ch linear driver IC with stacked current-reuse architecture in 65nm CMOS for beyond-400Gb/s coherent optical transmitters," in *Proc. IEEE Int. Solid-State Circuits Conf.*, 2020, pp. 212–214.
- [24] "Aerodiode model 3 (O-band) DFB laser," 2023. Accessed: May 11, 2023. [Online]. Available: <https://www.aerodiode.com/product/1310-nm-laser-diode>
- [25] F. Chang and R. Chen, "Relative cost analysis on IMDD vs coherent for 800G-LR," IEEE P802.3df Task Force Meeting, 2022. Accessed: May 20, 2023. [Online]. Available: [https://www.ieee802.org/3/df/public/22\\_11/chang\\_3df\\_01\\_2211.pdf](https://www.ieee802.org/3/df/public/22_11/chang_3df_01_2211.pdf)
- [26] H. Li et al., "A 112 Gb/s PAM4 CMOS optical receiver with sub-pJ/bit energy efficiency," in *Proc. IEEE Opt. Interconnects Conf.*, 2019, pp. 1–2.
- [27] Y. Segal et al., "A 1.41 pJ/b 224Gb/s PAM-4 SerDes receiver with 31dB loss compensation," in *Proc. IEEE Int. Solid-State Circuits Conf.*, 2022, pp. 114–116.